Effects of Helium Ion Exposure on the Single-Photon Sensitivity of MgB_2 and NbN Detectors

Emma Batson, Francesca Incalza, Matteo Castellani, Marco Colangelo, Ilya Charaev*, Andreas Schilling*, Sergey Cherednichenko*, Karl K. Berggren*

***Abstract*—Improving the scalability, reproducibility, and operating temperature of superconducting nanowire single photon detectors (SNSPDs) has been a major research goal since the devices were first proposed. The recent innovation of helium-ion irradiation as a post-processing technique for SNSPDs could enable high detection efficiencies to be more easily reproducible, but is still poorly understood. Additionally, fabricating detectors at micron-wide scales from high-T_C materials could improve scalability and operating temperature, respectively. At the same time, fabrication of successful devices in wide wires and from higher-T_C materials like magnesium diboride has proven challenging. In this work, we compare helium ion irradiation in niobium nitride and magnesium diboride detectors with different material stacks in order to better understand the mechanics of irradiation and practical implications of encapsulating layers on effective dose. We examine the effects of experimental effective dose tests and compare these results to the damage per ion predicted by simulations in corresponding material stacks. In both materials, irradiation results in an increase in count rate, though for niobium nitride this increase has not fully saturated even at the highest tested dose of 2.6×10^{17} ions/cm^2, while for resist-encapsulated magnesium diboride even the lowest tested dose of 1×10^{15} ions/cm^2 appears higher than optimal. Our results demonstrate the general applicability of helium ion irradiation to vastly different devices and material stacks, albeit with differing optimal doses, and show the reproducibility and effectiveness of this post-processing technique in significantly improving SNSPD efficiency.**

***Index Terms*—Magnesium diboride, niobium nitride, helium ion irradiation, SNSPD.**

I. Introduction

SINGLE photon sensitivity is critical in many low-signal applications such as biological imaging [1], [2], dark matter detection [3], and exoplanet search [4]. Superconducting nanowire single-photon detectors (SNSPDs) are promising candidates for these applications, having the potential to combine high sensitivity well into the infrared [4]–[6] with near-perfect detection efficiency [7], [8], low dark count rate [3], [9], and fast reset times [10]. However, these devices are usually fabricated in sputtered polycrystalline or amorphous superconducting materials in the nitride and silicide families such as niobium nitride (NbN). As a result, they only achieve high performance metrics at operating temperatures around 1 K due to the low gap and critical temperature of such materials [11]. Additionally, achieving large active area while maintaining performance can be difficult in nanowire devices due to effects such as the greater probability of constrictions in longer wires [12] and current crowding in densely meandered wires [13].

Recent advancements in the quality of superconducting materials with higher transition temperatures such as magnesium diboride (MgB_2) [14] and the fabrication of superconducting microwire single photon detectors [15] provide potential solutions to these problems. Improved materials with higher transition temperatures could open a path to SNSPDs with higher operating temperatures [16]. Also, because a wide wire can cover a larger area with a shorter length, large-area micrometer-wide detectors can have fewer constrictions and a faster reset time than comparably large narrow devices.

Furthermore, renewed interest in ion irradiation of superconducting thin films has opened the possibility of modifying devices post-fabrication to improve their properties, mildly suppressing switching current in exchange for significantly higher detection efficiency [17], [18]. In fact, single photon detection has now been observed in helium-irradiated, micron-wide magnesium diboride (MgB_2) SPDs at 20 K [19].

Although all this recent work is promising, truly scalable, high-operating-temperature, large-area devices will require fabrication that is robust, reproducible, and fast. It is also critical to develop a better understanding of the underlying mechanisms by which ion irradiation improves device performance in order to control and predict the associated effects, including mitigating any undesirable side effects. To this end, we chose to study and compare the effects of helium ion irradiation in both wide-wire MgB_2 devices as well as more conventional nanowire NbN devices. By directly comparing the effects of irradiation in such different devices, we hope to better isolate the dynamics of helium ion irradiation and its

Manuscript received November 30, 2023. We thank Yang Yu for help in preparing the STEM lamella and Aubrey Penn for assistance obtaining the STEM data. We also thank Prof. Luqiao Liu for use of ion milling facilities. Work was completed in part in MIT.nano facilities. Work was supported by the NSF as part of the CQN program under Grant No. EEC1941583. E. Batson acknowledges the National Science Foundation Graduate Research Fellowship under Grant No. 2141064. M. Colangelo acknowledges support from the Claude E. Shannon award.

E. Batson, F. Incalza, M. Castellani, M. Colangelo, and K. K. Berggren are with the Department of Electrical Engineering and Computer Science, Massachusetts Institute of Technology, Cambridge, MA, USA.

M. Colangelo is now with Northeastern University, Cambridge, MA, USA.

I. Charaev and A. Schilling are with the Physics Institute, University of Zurich, Zurich, Switzerland.

S. Cherednichenko is with the Department of Microtechnology and Nanoscience, Chalmers University of Technology, Gothenburg, Sweden.

*co-corresponding authors

role in device performance.

In this work, we further the understanding of the effects of helium ion irradiation through simulation and STEM imaging, confirm key results in ion-modified magnesium diboride wide-wire detectors and nanowire niobium nitride detectors, and also present modified fabrication techniques to improve the reliability and speed of fabrication in magnesium diboride.

II. Methods

In this section, we describe the simulation techniques used to develop an understanding of the ion implantation effects, as well as the fabrication methods used to produce devices in niobium nitride and magnesium diboride, including helium ion irradiation. Finally, we describe the readout electronics used in photon detection measurements.

A. Simulation and Material Characterization

In our study, damage per ion was estimated by using the TRIM [20] "quick calculations" mode to simulate vacancies in a target material stack resulting from irradiation with 30 keV helium ions. Although TRIM in this mode has some limitations, typically underestimating actual damage per ion [21], this mode should be sufficient for qualitative comparisons of irradiation damage across different film stacks. We create models of three different material stacks: an NbN stack, consisting of 20 nm NbN, 300 nm SiO_2, and an arbitrary depth of the silicon substrate; an MgB_2 stack without resist on top, consisting of 2 nm amorphous silicon encapsulation, 2 nm MgO presumed to have formed on top, 7 nm MgB_2, and an arbitrary depth of SiC; and an MgB_2 stack with resist on top, identical to the former but with 200 nm of a resist model based on the properties of PMMA [22] on top of the amorphous silicon. These stacks correspond to those on which we fabricated our devices.

We also used STEM with EDS to characterize the crystallinity of a lamella prepared with focused ion beam milling from a device after irradiation, and used a SEM to study the effects of helium ion irradiation on the film surfaces.

B. Fabrication Techniques

Niobium nitride (NbN) film was deposited on a thermal-silicon-oxide on a 1 cm $\times$ 1 cm silicon substrate with 300-nm-thick oxide using an AJA sputtering system set to 160 W peak power. We used positive tone resist ZEP-530A (Zeon) spun at 5000 rpm for 60 s and baked at 180 °C for 120 s. Devices were patterned with electron-beam lithography (Elionix ELS-F125). Then, we developed the resist in o-xylene at 5 °C for 60 s and rinsed the samples in isopropanol (IPA) for 30 s. Pattern transfer was performed via reactive ion etching (RIE) based on CF_4 at 50 W. Afterward we rinsed the chips in N-Methyl-2-pyrrolidone (NMP) at 70 °C for 3 hr.

Magnesium diboride (MgB_2) film was deposited on a 1 cm $\times$ 1 cm silicon carbide substrate via hybrid physical-chemical vapor deposition (HPCVD) [23], [24]. The film used in this work was deposited for 85 s, corresponding to an estimated thickness of 7 nm. Before nanofabrication, the films were encapsulated with about 2 nm amorphous silicon sputtered in the AJA. Electron-beam lithography was similar to that in NbN, except we used a slower spin speed for the ZEP of 4000 rpm, and we spun on a charge dissipation layer of Electra 92 (Allresist) at 2000 rpm for 60 s and baked it at 90 ° C for 60 s. Pattern transfer was performed via argon ion milling with 8 sccm argon and beam voltage and current of 250 V and 13 mA with a 30 ° angle from normal. Chips were not soaked in NMP for resist removal due to magnesium diboride's sensitivity to long exposures to solvents [25]. Based on ellipsometric measurements, we estimated that about 200 nm of resist remain after milling.

Once the devices were fabricated, we scanned over the entire area of selected devices with a Zeiss Orion helium ion microscope (HIM) set to 30 keV. Use of the largest available aperture and higher pressures allowed us to achieve currents of over 100 pA. Doses were calculated by the starting current multiplied by total dwell time on the device area. The beam current tended to drift downward over the course of a scan, leading to potential uncertainties and nonuniformities in actual dose for larger devices. Areal dose densities (doses) were swept from 1×10^{15} ions/cm^2 - 5×10^{16} ions/cm^2 for 100 µm $\times$ 200 µm 1-micron-wide magnesium diboride meanders, and from 1×10^{14} ions/cm^2 - 2.6×10^{17} ions/cm^2 for a 5 µm $\times$ 5 µm 100 nm wide niobium nitride wires.

C. Experimental Setup

Niobium nitride devices were measured in a custom built dip probe in a helium dewar. Magnesium diboride devices were measured in a two-stage cryostat with only the first stage running, with a base temperature of 3 K for this mode of operation, which could be controllably heated up to 20 K. The micron-scale magnesium diboride wires are known to have a low kinetic inductance compared to niobium nitride, due to both the underlying material properties [14] and the relatively short meander lengths of wide wires. This low inductance required use of an additional cold-stage inductive and resistive shunt to prevent latching. Magnesium diboride detectors were illuminated with a 1550 nm laser through a fiber-optic cable with a variable attenuator, while niobium nitride detectors were illuminated with a 780 nm laser.

III. Results and Discussion

In this section, we first discuss the results of irradiation simulations and the characterization of irradiated material, then the results of MgB_2 wide-wire device irradiation, and then the results of NbN SNSPD irradiation. We then relate the performance of these devices to the simulation and characterization results.

A. Irradiation Dynamics in Different Stacks

In Figure 2, we analyze the simulated results of ion irradiation in the stacks of NbN, MgB_2, and MgB_2 encapsulated with resist through SRIM simulations. The MgB_2 and encapsulated MgB_2 simulations were used to investigate the slowing effect of the resist on the helium ions. As seen

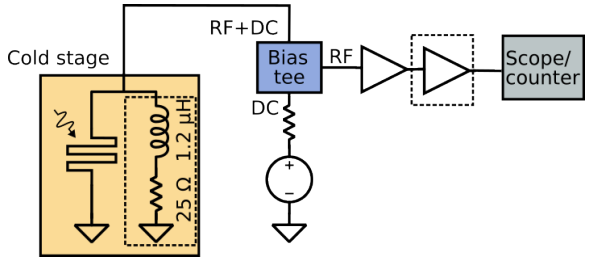

Fig. 1. The readout electronics setups for magnesium diboride wires and niobium nitride wires were nearly identical, with optional components shown in dashed lines. A cold-stage off-chip shunt was necessary to prevent latching in the wide magnesium diboride wires. Bias current was provided by a voltage source and a 1 kΩ resistor for the wide magnesium diboride wires or a 10 kΩ resistor for the narrow NbN wires. At low temperatures in the wide wires, only one stage of amplification was necessary. Detectors were illuminated with a 1550 nm laser (magnesium diboride) or 780 nm laser (niobium nitride) through a fiber-optic cable.

in Figures 2(a), (b), and (c), the distribution of vacancies produced per ion over the depth differs significantly between these stacks. Depths corresponding to the superconducting film layer are highlighted in gold. The MgB_2 encapsulated with resist (Figure 2(c) sees significantly more average vacancies per helium ion than MgB_2 without resist (Figure 2(b). Adding up the total number of vacancies per ion over the whole depth, we expect about twice as many total vacancies per ion to occur in resist-encapsulated MgB_2. We can therefore expect magnesium diboride capped with resist to receive a higher effective dose per ion than a clean magnesium diboride surface. Also, the simulations show that NbN receives a dose similar to that of MgB_2 capped with resist, which is likely due to the relatively large density of the NbN.

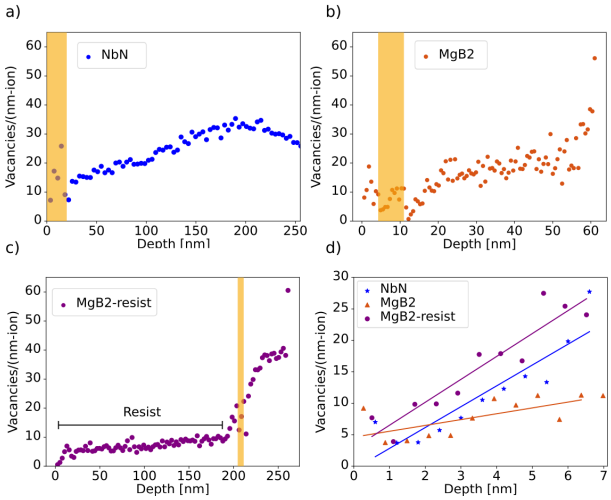

Fig. 2. SRIM simulations of the (a) NbN stack (20 nm NbN, 300 nm SiO_2, arbitrary depth of Si), (b) the magnesium diboride stack without resist (2 nm amorphous Si, 2 nm MgO, 7 nm MgB_2, arbitrary depth of SiC), and (c) the magnesium diboride stack with 200 nm resist on top. Superconducting film layers are highlighted in gold. (d) Simulated points inside the superconducting film layers for the three stacks. A linear regression is drawn to guide the eye. The total number of average vacancies per ion induced in the magnesium diboride layer is predicted to be nearly doubled by the presence of resist on top.

In order to better understand the effects of helium ion irradiation on actual devices, we prepared a TEM lamella from a 1-μm-wide MgB_2 wire irradiated to 1×10^{16} ions/cm^2. This dose had proven too high, and the device was no longer superconducting after the irradiation. Wires irradiated to this level became insulating, with a normal-state resistance too high to measure with a standard multimeter. A bright-field micrograph, shown in Figure 3 with bright and dark levels adjusted for clarity, reveals significant but non-uniform amorphization of the magnesium diboride film. Although the silicon carbide remains single-crystalline everywhere, the magnesium diboride is single-crystalline in the right side of this field of view but amorphous in the left side. EDS analysis (Supplement 2.1) confirmed that the amorphous region was also magnesium diboride, and suggested that the crystalline interfacial layer was also magnesium rich. This data supports the idea that helium ion irradiation creates amorphizing vacancies, and that focused-ion methods such as helium ion microscopy may have problems with non-uniformity.

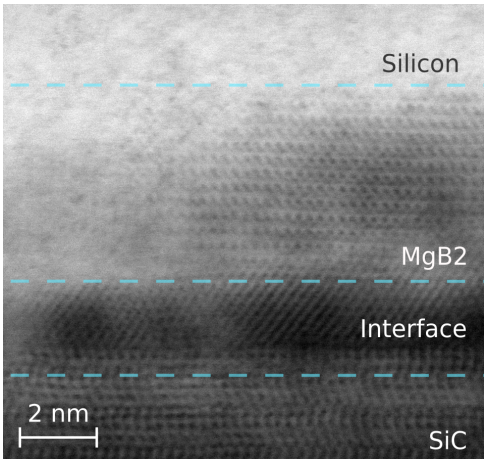

Fig. 3. STEM showing a lamella cross-section of a 1-μm-wide MgB_2 wire irradiated to 1×10^{16} ions/cm^2. This is the bright-field micrograph, with bright and dark levels adjusted for clarity. The silicon carbide is single-crystalline everywhere in this micrograph, allowing for single-atomic resolution. To the left of the field of view, the magnesium diboride is also single-crystalline, since it was grown epitaxially on the silicon carbide. However, to the right of the field of view, the magnesium diboride has been amorphized by the ion irradiation. According to EDS, the interfacial layer is also magnesium-rich.

SEM images of the surface of a similar device irradiated to 5×10^{15} ions/cm^2, shown in Figure 4(a), also indicate non-uniformity. Around the device area, which is the irradiated region, the encapsulating resist is wrinkled and stressed. Within the irradiated region, bubbles up to 500 nm in diameter formed preferentially near the edges of the wires. The resist is flexible compared to the MgB_2, and the bubbling may not extend to the superconducting layer below. Still, the bubbles indicate non-uniformities and dynamics of the irradiation process beyond what SRIM can simulate, suggesting a need for further study.

B. *Irradiated MgB_2 Wide-Wire Detectors*

We expect that an optimal helium irradiation dose exists, at which total count rate is maximized with little effect on switching current and transition temperature, in MgB_2 [19] and NbN [17]. For this dose or lower, our irradiated

devices should have properties similar to our non-irradiated devices. For MgB_2 with a resist encapsulation layer, however, we observe that a 1-μm-wide wire irradiated to the lowest tested dose, 1×10^{15} ions/cm^2, has its switching current suppressed from about 1-2 mA to about 215 μA, 10-20% of its original value. Room-temperature resistances and 3 K switching currents are given for this and several comparable non-irradiated wires in Table I. Switching current curves at 3 K and 10 K are shown in Figure 4(b).

Additionally, the transition temperature of the irradiated device was suppressed from about 35 K to about 20 K, 60% of its original value. Wires irradiated to higher levels were no longer useful devices after treatment. Devices irradiated to 5×10^{15} ions/cm^2 showed room-temperature resistances of over 1 MΩ; one was superconducting with a 3 K switching current of only 5 μA, while the other remained in the normal state at 3 K. Devices irradiated to 1×10^{16} ions/cm^2 or higher failed to register a finite resistance on a standard multimeter at room temperature or at 3 K. In contrast, Charaev et al. [19] found a dose of 5×10^{15} ions/cm^2 to be optimal for MgB_2 without resist capping for similar films with similar fabrication techniques. By comparison, even the 1×10^{15} ions/cm^2-dosed wire appears to be effectively dosed moderately beyond the optimum point, despite the low integrated total dose. Based on SRIM simulations shown in Figure 2, we attribute this to an increased vacancy generation rate per helium ion caused by deceleration of the ions in the resist layer on top.

Device ID	R(RT) [kΩ]	I_{sw} (3 K) [mA]
a1	385	2.1
e1	457	1.2
h1	410	1.9
d1 (irradiated 1e15)	1100	0.21
i1 (irradiated 5e15)	2000	0.005

TABLE I
ROOM TEMPERATURE RESISTANCE AND SWITCHING CURRENT OF 1-μm-WIDE WIRES IN MgB_2.

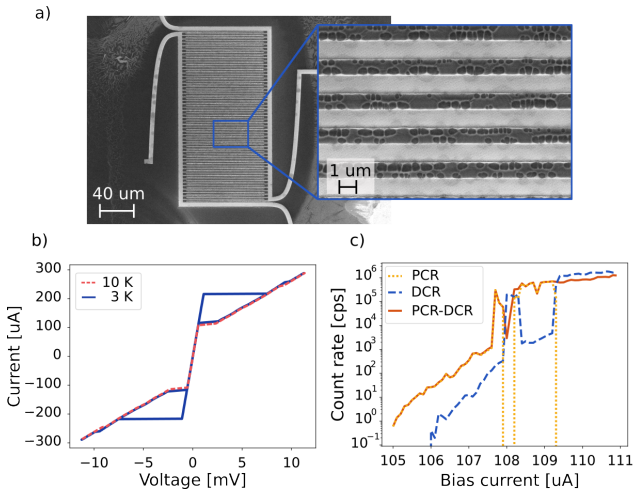

Fig. 4. (a) SEM image of a 1-μm-wide MgB_2 wire irradiated to 5×10^{15} ions/cm^2. (right inset) Helium visibly bubbles up through the resist on the film surface. (b) $I-V$ curves of a 1-μm-wide MgB_2 wire irradiated to 1×10^{15} ions/cm^2 at 3 K (blue dashed line) and 10 K (orange solid line), measured with the shunt. The switching current at 3 K, about 215 μA, is about 20% the pre-irradiation value of 1 mA. Hysteresis has nearly vanished at 10 K, the highest temperature at which any pulses were observed. (c) Light and dark count rates of the 1-μm-wide MgB_2 wire irradiated to 1×10^{15} ions/cm^2 as a function of bias current at 10 K. As can occur in NbN wide-wire devices [26], counting is only seen at biases very close to the switching current. The maximum true count rate is about 1 kcps. Rapid pulses that show the periodic behavior of relaxation oscillations on oscilloscope readout are seen in both the light and dark count curves at rates up to 1 MHz. This could indicate poor sensitivity of the device due to over-irradiation, but the preservation of rapid dynamics in the material.

Nonetheless, the irradiated device, which originally demonstrated no sensitivity to light beyond a thermal suppression of switching current at high laser powers, became able to detect photons up to 10 K post-irradiation. Linearity checks (provided in Supplemental Information) indicated multi-photon sensitivity. As shown in Figure 4(b), 10 K, about half the transition temperature, was the highest temperature at which the transition to the normal state was sharp, and perhaps still slightly hysteretic. Below 10 K, there was clear hysteresis, but above 10 K, the transition softened. In Figure 4(c), we see that counts only occurred at bias currents very close to the switching current, a feature that has also been observed in wide-wire geometries in NbN [26]. At 10 K, a count rate up to 1 kcps with dark counts of 100 cps was observed. Near the switching current, the apparent count rate jumps up by orders of magnitude to 1 MHz and pulses become periodic, suggesting relaxation oscillations [27].

Interestingly, at intermediate levels of bias current (between about 107.5 μA - 108 μA for PCR, or 108 μA - 109.5 μA for DCR), we sometimes observe short (> 1 s) bursts of periodic pulses, and sometimes observe typical counting behavior. At these intermediate bias levels, therefore, the counting period sometimes captures a burst of high-frequency oscillations and sometimes does not. Similar behavior is seen in both the light and dark count curves, and was also observed in dark count curves taken prior to irradiation. These high-frequency oscillating behaviors indicate that the irradiated device material can still support high-frequency dynamics, even though it does not see light counts at such high rates. Possibly in the overdosed wire, only a small fraction of the wire was able to participate in detection, thus limiting the count rate.

C. Irradiated NbN SNSPDs

Our results irradiating niobium nitride SNSPDs were different from MgB_2 in several respects: (1) the devices were single-photon sensitive; (2) the devices were photosensitive both before and after irradiation; and (3) the devices were tolerant (both superconducting and photosensitive) up to the highest tested dose.

An SEM of an example NbN device is shown in Figure 5(a). The devices were single-photon sensitive with low dark count rates that did not show a clear dependence on helium-ion dose. In the results of Zhang et al. [17], the switching current of NbN devices was roughly halved and the count rate began to decrease after exposure to 1×10^{16} ions/cm^2. In contrast, our devices still showed improved count rate and roughly 85% the original switching current even at a dose of 2.6×10^{17} ions/cm^2, although they did not saturate, as shown in Figure 5(c). Given the thicker films used in our devices, a

less saturating PCR curve may be expected, and this points to a need for further experiments with saturated devices in the future. However, unlike our resist-encapsulated MgB_2 devices or Zhang's NbN SNSPDs, it seems that even higher doses than those we tested could have a positive effect. Over the tested dose range, the maximum count rate of our devices increased monotonically up to $7\times$ the maximum rate for a non-irradiated device, as shown in Figure 5(b), though saturation at higher doses still implies an optimal value.

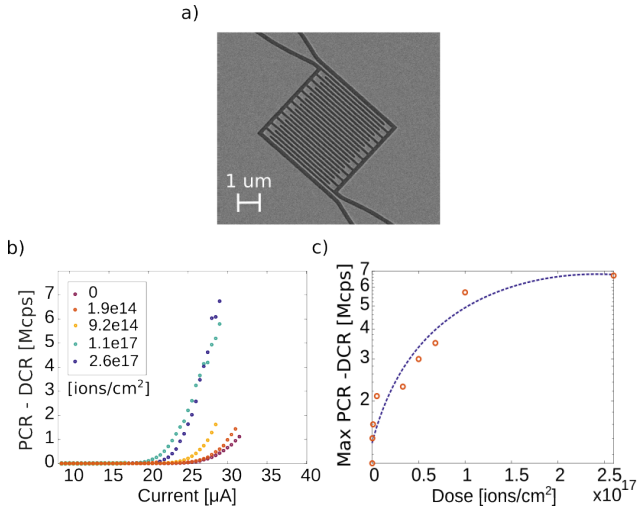

Fig. 5. (a) SEM of an NbN SNSPD before helium ion irradiation. (b) Maximum count rate vs. helium ion dose for NbN SNSPDs, with a line drawn to guide the eye. The maximum count rate increases monotonically at least up to a dose of 2.6×10^{17} ions/cm^2, and is about $7\times$ greater for the highest-dosed device compared to the non-irradiated devices. Measurements are taken in a helium dewar at 4.2 K. (c) PCR - DCR vs bias current for irradiated devices. The switching current decreases moderately with increased irradiation. The most-irradiated device has about 85% the switching current of the non-irradiated device.

We can conclude from SRIM simulations that NbN, which is 3.3 times denser than MgB_2 [28], [29], accumulates damage under helium ion irradiation at a rate comparable to that of resist-encapsulated MgB_2. However, NbN appears to not only tolerate but be improved by doses orders of magnitude higher than those that destroy superconductivity in MgB_2. This improvement may indicate a relationship between the optimal effective dose for maximizing detection efficiency and the intrinsic defects present in a newly fabricated device. Other than density, which is accounted for in SRIM, a major difference between our NbN and MgB_2 films is the original crystallinity. Sputtered NbN is finely polycrystalline with many grain boundaries, while MgB_2 grows epitaxially on SiC. It may be that films like NbN, with a higher intrinsic defect, density require a higher helium ion dose to see its benefits.

IV. Conclusions

Our results show that helium ion irradiation in the appropriate dose can significantly increase maximum count rate of SNSPDs with the cost of only a small decrease in transition temperature, a modest decrease in switching current, and insignificant impact on dark count rate. Comparison with existing literature indicates that these results are robust and easy to reproduce across metallic superconductors as different as sputtered polycrystalline niobium nitride and epitaxially grown HPCVD magnesium diboride. However, our results also indicate that the actual optimum dose can vary by orders of magnitude depending on encapsulation conditions, which can be predicted qualitatively by SRIM, and depending on other material factors which are not captured by SRIM.

Adding encapsulation layers that slow down helium ions before their interaction with the electronic layer increases the effective dose for a given ion dose. This result is predicted by SRIM, which shows about twice as many vacancies per ion in MgB_2 in the presence of a resist encapsulation layer, and confirmed by our experiments, which show greater degradation of encapsulated MgB_2 compared to bare MgB_2 in the literature [19]. We observed heavy amorphization of the encapsulated MgB_2 film at a dose of 1×10^{16} ions/cm^2 in STEM. We also saw that irradiation to 1×10^{15} ions/cm^2 improved device sensitivity but caused significant reduction in critical temperature and switching current. If correctly accounted for, this increase in effective dose can be used to speed up irradiation damage for a more scalable process.

Additionally, we observed benefits from irradiation of NbN to significantly higher doses than: (1) our MgB_2, (2) MgB_2 in the literature [19], or (3) NbN in the literature [17]. This difference suggests a dependence of optimal dose on intrinsic properties of the starting material such as intrinsic defect density, and further emphasizes the importance of experimental dose tests for obtaining the greatest effect of helium ion irradiation.

Although our experiments do not conclusively indicate why irradiation increases SNSPD detection efficiency, we do observe that increased count rate always comes at the cost of a lowered switching current. Typically, the switching current of a pre-irradiated device is limited by a small number of "weak points," e.g. at sharp turns or grain boundaries, which produce the majority of dark counts and are not necessarily uniformly distributed throughout the device [30], [31]. The lowered switching current of an irradiated device may be limited by new weak points caused by irradiation damage, which are expected to be denser and more uniformly distributed than the intrinsic weak points. As a result, when the irradiated device is biased near its switching current, these dense and uniformly distributed weak points all become very sensitive, whereas before irradiation only a few weak points with uncontrolled placement were comparably sensitive. In this scenario, irradiation would increase detection efficiency by increasing the number of sites that participate in detection near the device switching current. Further experiments on the spatial distribution of weak points in irradiated devices could clarify whether this is a plausible mechanism for the improved sensitivity we observed. On the other hand, Charaev et al. [19] observed a decrease in the retrapping current of irradiated devices, which could indicate other mechanisms. However, our devices were too heavily irradiated to observe such an effect, as the switching currents of the irradiated devices were lower than the pre-irradiation retrapping currents.

V. References Section

References

[1] F. Wang, F. Ren, Z. Ma, L. Qu, R. Gourgues, C. Xu, A. Baghdasaryan, J. Li, I. E. Zadeh, J. W. N. Los, A. Fognini, J. Qin-Dregely, and H. Dai, "In vivo non-invasive confocal fluorescence imaging beyond 1,700 nm using superconducting nanowire single-photon detectors," *Nat. Nanotechnol.*, vol. 17, pp. 653–660, June 2022. Number: 6 Publisher: Nature Publishing Group.

[2] C.-W. Lin, S. Huang, M. Colangelo, C. Chen, F. N. C. Wong, Y. He, K. K. Berggren, and A. M. Belcher, "Surface Plasmon Enhanced Upconversion Fluorescence in Short-Wave Infrared for In Vivo Imaging of Ovarian Cancer," *ACS Nano*, vol. 16, pp. 12930–12940, Aug. 2022. Publisher: American Chemical Society.

[3] J. Chiles, I. Charaev, R. Lasenby, M. Baryakhtar, J. Huang, A. Roshko, G. Burton, M. Colangelo, K. Van Tilburg, A. Arvanitaki, S. W. Nam, and K. K. Berggren, "New Constraints on Dark Photon Dark Matter with Superconducting Nanowire Detectors in an Optical Haloscope," *Phys. Rev. Lett.*, vol. 128, p. 231802, June 2022. Publisher: American Physical Society.

[4] E. E. Wollman, V. B. Verma, A. B. Walter, J. Chiles, B. Korzh, J. P. Allmaras, Y. Zhai, A. E. Lita, A. N. McCaughan, E. Schmidt, S. Frasca, R. P. Mirin, S.-W. Nam, and M. D. Shaw, "Recent advances in superconducting nanowire single-photon detector technology for exoplanet transit spectroscopy in the mid-infrared," *JATIS*, vol. 7, p. 011004, Jan. 2021. Publisher: SPIE.

[5] V. B. Verma, B. Korzh, A. B. Walter, A. E. Lita, R. M. Briggs, M. Colangelo, Y. Zhai, E. E. Wollman, A. D. Beyer, J. P. Allmaras, H. Vora, D. Zhu, E. Schmidt, A. G. Kozorezov, K. K. Berggren, R. P. Mirin, S. W. Nam, and M. D. Shaw, "Single-photon detection in the mid-infrared up to 10 μm wavelength using tungsten silicide superconducting nanowire detectors," *APL Photonics*, vol. 6, p. 056101, May 2021.

[6] M. Colangelo, A. B. Walter, B. A. Korzh, E. Schmidt, B. Bumble, A. E. Lita, A. D. Beyer, J. P. Allmaras, R. M. Briggs, A. G. Kozorezov, E. E. Wollman, M. D. Shaw, and K. K. Berggren, "Large-Area Superconducting Nanowire Single-Photon Detectors for Operation at Wavelengths up to 7.4 μm," *Nano Lett.*, vol. 22, pp. 5667–5673, July 2022. Publisher: American Chemical Society.

[7] D. V. Reddy, R. R. Nerem, S. W. Nam, R. P. Mirin, and V. B. Verma, "Superconducting nanowire single-photon detectors with 98% system detection efficiency at 1550 nm," *Optica, OPTICA*, vol. 7, pp. 1649–1653, Dec. 2020. Publisher: Optica Publishing Group.

[8] J. Chang, J. W. N. Los, J. O. Tenorio-Pearl, N. Noordzij, R. Gourgues, A. Guardiani, J. R. Zichi, S. F. Pereira, H. P. Urbach, V. Zwiller, S. N. Dorenbos, and I. Esmaeil Zadeh, "Detecting telecom single photons with 99.5-2.07+0.5% system detection efficiency and high time resolution," *APL Photonics*, vol. 6, p. 036114, Mar. 2021.

[9] H. Shibata, K. Fukao, N. Kirigane, S. Karimoto, and H. Yamamoto, "SNSPD With Ultimate Low System Dark Count Rate Using Various Cold Filters," *IEEE Transactions on Applied Superconductivity*, vol. 27, pp. 1–4, June 2017. Conference Name: IEEE Transactions on Applied Superconductivity.

[10] C. Autebert, G. Gras, E. Amri, M. Perrenoud, M. Caloz, H. Zbinden, and F. Bussières, "Direct measurement of the recovery time of superconducting nanowire single-photon detectors," *Journal of Applied Physics*, vol. 128, p. 074504, Aug. 2020.

[11] A. Banerjee, L. J. Baker, A. Doye, M. Nord, R. M. Heath, K. Erotokritou, D. Bosworth, Z. H. Barber, I. MacLaren, and R. H. Hadfield, "Characterisation of amorphous molybdenum silicide (MoSi) superconducting thin films and nanowires," *Supercond. Sci. Technol.*, vol. 30, p. 084010, July 2017. Publisher: IOP Publishing.

[12] A. J. Kerman, E. A. Dauler, J. K. W. Yang, K. M. Rosfjord, V. Anant, K. K. Berggren, G. N. Gol'tsman, and B. M. Voronov, "Constriction-limited detection efficiency of superconducting nanowire single-photon detectors," *Applied Physics Letters*, vol. 90, p. 101110, Mar. 2007.

[13] H. L. Hortensius, E. F. C. Driessen, T. M. Klapwijk, K. K. Berggren, and J. R. Clem, "Critical-current reduction in thin superconducting wires due to current crowding," *Applied Physics Letters*, vol. 100, p. 182602, May 2012.

[14] S. Cherednichenko, N. Acharya, E. Novoselov, and V. Drakinskiy, "Low kinetic inductance superconducting MgB2 nanowires with a 130 ps relaxation time for single-photon detection applications," *Supercond. Sci. Technol.*, vol. 34, p. 044001, Feb. 2021. Publisher: IOP Publishing.

[15] J. Chiles, S. M. Buckley, A. Lita, V. B. Verma, J. Allmaras, B. Korzh, M. D. Shaw, J. M. Shainline, R. P. Mirin, and S. W. Nam, "Superconducting microwire detectors based on WSi with single-photon sensitivity in the near-infrared," *Applied Physics Letters*, vol. 116, p. 242602, June 2020.

[16] I. Charaev, D. A. Bandurin, A. T. Bollinger, I. Y. Phinney, I. Drozdov, M. Colangelo, B. A. Butters, T. Taniguchi, K. Watanabe, X. He, O. Medeiros, I. Božović, P. Jarillo-Herrero, and K. K. Berggren, "Single-photon detection using high-temperature superconductors," *Nat. Nanotechnol.*, vol. 18, pp. 343–349, Apr. 2023. Number: 4 Publisher: Nature Publishing Group.

[17] W. Zhang, Q. Jia, L. You, X. Ou, H. Huang, L. Zhang, H. Li, Z. Wang, and X. Xie, "Saturating Intrinsic Detection Efficiency of Superconducting Nanowire Single-Photon Detectors via Defect Engineering," *Phys. Rev. Applied*, vol. 12, p. 044040, Oct. 2019. Publisher: American Physical Society.

[18] K. Kohopää, A. Ronzani, R. N. Jabdaraghi, A. Bera, M. Ribeiro, D. Hazra, E. Mykkänen, J. Senior, M. Prunnila, J. Govenius, J. S. Lehtinen, and A. Kemppinen, "Wafer-scale method for amorphizing superconducting thin films," Mar. 2023. arXiv:2303.11202 [cond-mat].

[19] I. Charaev, E. K. Batson, S. Cherednichenko, K. Reidy, V. Drakinskiy, Y. Yu, S. Lara-Avila, J. D. Thomsen, M. Colangelo, F. Incalza, K. Ilin, A. Schilling, and K. K. Berggren, "Single-photon detection using large-scale high-temperature MgB$_2$ sensors at 20 K," Aug. 2023. arXiv:2308.15228 [cond-mat].

[20] J. Ziegler, "SRIM and TRIM."

[21] W. J. Weber and Y. Zhang, "Predicting damage production in monoatomic and multi-elemental targets using stopping and range of ions in matter code: Challenges and recommendations," *Current Opinion in Solid State and Materials Science*, vol. 23, p. 100757, Aug. 2019.

[22] PubChem, "Methyl methacrylate."

[23] X. X. Xi, A. V. Pogrebnyakov, S. Y. Xu, K. Chen, Y. Cui, E. C. Maertz, C. G. Zhuang, Q. Li, D. R. Lamborn, J. M. Redwing, Z. K. Liu, A. Soukiassian, D. G. Schlom, X. J. Weng, E. C. Dickey, Y. B. Chen, W. Tian, X. Q. Pan, S. A. Cybart, and R. C. Dynes, "MgB2 thin films by hybrid physical–chemical vapor deposition," *Physica C: Superconductivity*, vol. 456, pp. 22–37, June 2007.

[24] E. Novoselov, N. Zhang, and S. Cherednichenko, "Study of MgB2 Ultrathin Films in Submicron Size Bridges," *IEEE Transactions on Applied Superconductivity*, vol. 27, pp. 1–5, June 2017. Conference Name: IEEE Transactions on Applied Superconductivity.

[25] Y. Cui, J. Jones, A. Beckley, R. Donovan, D. Lishego, E. Maertz, A. Pogrebnyakov, P. Orgiani, J. Redwing, and X. Xi, "Degradation of MgB/sub 2/ thin films in water," *IEEE Transactions on Applied Superconductivity*, vol. 15, pp. 224–227, June 2005. Conference Name: IEEE Transactions on Applied Superconductivity.

[26] O. Medeiros, *Investigation of Thin Film Supercurrent and Photodetection in Wide Niobium Nitride Wires*. Thesis, Massachusetts Institute of Technology, May 2022. Accepted: 2022-08-29T15:56:10Z.

[27] E. Toomey, Q.-Y. Zhao, A. N. McCaughan, and K. K. Berggren, "Frequency Pulling and Mixing of Relaxation Oscillations in Superconducting Nanowires," *Phys. Rev. Appl.*, vol. 9, p. 064021, June 2018. Publisher: American Physical Society.

[28] "Magnesium diboride $\geq$99% (metals basis)."

[29] "Niobium nitride, Thermo Scientific Chemicals, Quantity: 10 g | Fisher Scientific."

[30] J. R. Clem and K. K. Berggren, "Geometry-dependent critical currents in superconducting nanocircuits," *Phys. Rev. B*, vol. 84, p. 174510, Nov. 2011. Publisher: American Physical Society.

[31] V. Andreev, A. Semenov, N. Manova, V. Seleznev, S. Svyatodukh, A. Divochiy, P. Morozov, and G. Goltsman, "Dark Counts in SNSPD Studied With Spatial Resolution," *IEEE Transactions on Applied Superconductivity*, pp. 1–5, 2024. Conference Name: IEEE Transactions on Applied Superconductivity.